This is a repository copy of *NIR emission studies and dielectric properties of Er(3+)-doped multicomponent tellurite glasses.*.

White Rose Research Online URL for this paper:
http://eprints.whiterose.ac.uk/97132/

Version: Accepted Version

NIR emission studies and dielectric properties of Er^{3+} -doped multicomponent tellurite glasses

M.S Sajna[a], Sunil Thomas[a], C. Jayakrishnan[b], Cyriac Joseph[a], P.R Biju[a], N.V Unnikrishnan[a]

[a]School of Pure & Applied Physics, Mahatma Gandhi University, Kottayam - 686 560, India

[b]Institute for Materials Research, University of Leeds, UK

*Tel: +91 9745047850, Email: nvu100@yahoo.com

Abstract

Multicomponent tellurite glasses containing altered concentrations of Er$_2$O$_3$ (ranging from 0 to 1 mol%) were prepared by the standard melt quenching technique. Investigations through energy dispersive X-ray spectroscopy (EDS), Raman scattering spectroscopy, FTIR spectroscopy, NIR emission studies and dielectric measurement techniques were done to probe their compositional, structural, spectroscopic and dielectric behaviour. The influence of erbium ion concentration on the infrared emission (~1.53 μm) of these glasses and their respective lifetimes were measured. From the measured capacitance and dissipation factor, the relative permittivity, dielectric loss and the conductivity were computed; which furnish the dielectric nature of the multicomponent tellurite glasses that depend on the frequency of the applied LCR meter. Assuming the ideal Debye behaviour as substantiated by Cole-Cole plot, an examination of the real and imaginary parts of impedance is performed. The power-law and Cole-Cole parameters were resolved for all the glass samples. From the assessment of the NIR emission analysis and dielectric properties of the glass samples, it is manifested that the Er^{3+} ion concentration has played a vital role in tuning the optical and dielectric properties and the 0.5 mol% Er^{3+} -doped glass is confirmed as the finest composition.

Keywords: Tellurite glass, Erbium, NIR emission, dielectric properties

1. Introduction

Studies on chalcogenide based glasses have drawn a great deal of attention to both industrial as well as academic researchers. These glasses have been extensively explored owing to their relevance in certain technological applications namely non-linear systems, optoelectronic devices, wave guiding applications and infrared telecommunication systems [1-4]. Tellurium dioxide is the material of preference for the present investigation through melt quench route, as it is one of the least explored chalcogen glass systems because of its toxicity and relatively high precursor cost. This material is beneficial both for direct application or being employed in the preparation of other device materials. Tellurite glasses were known to have reduced probability of multiphonon relaxation from the excited states of rare earths integrated in it compared with that of other glass hosts like silica [5]. It is also known to have a range of attracting features in various optical communication devices so as to meet the purpose of optical amplification [6]. Employing low phonon energy matrices like tellurite glass, it is possible to provide a suitable host for rare earths to minimize non-radiative losses. The scientific interest of tellurium oxide (TeO$_2$) based glasses arises on account of their various

distinctive properties like high refractive index (~ 2), large transmittance window (ranging from visible to infrared region), high dielectric constant and good chemical durability [7,8]

Multicomponent tellurite glasses merge the advantages of constituent glass formers. Even if these glass systems have several improved properties, the analysis and understanding of the experimental outcomes have been hampered largely by the complexity in structure of the glass matrix arising due to the incorporation of multiple glass formers. By opting multicomponent tellurite glasses, there evolves the possibility of formation of diverse structural sites. This reduces the adverse clustering of dopant species and it provides ground for adequate fluorescence emission [9]. It also combines the property of high rare earth ion solubility, which is important for developing Er^{3+} - doped amplifiers [6]. In order to accomplish the demand for large bandwidth needed for the wavelength division multiplexing systems, the optical properties of the Er^{3+} ions in different glass matrices have widely been studied. Erbium is known to be an interesting dopant as its intra-4f transition between the first excited state ($^4I_{13/2}$) to the ground state ($^4I_{15/2}$) causes luminescence at 1.53 μm, which is a standard wavelength in telecommunication. Er^{3+} -doped tellurite glasses possess large emission cross- section and broad emission bandwidth compared to other glass hosts, which recognize it as a noteworthy material for high performance fibre amplifiers [10].

Fabrication of high dielectric constant materials can afford higher charge storage densities provided that they exhibit lower dielectric losses. To understand the nature of conduction and the defect centres existing in the chalcogenide glass systems, the ac conductivity and dielectric properties provide a fundamental route. The dielectric studies along with some structural analysis give an idea on the structural aspects of the glasses. In the present investigation, in order to satisfy the requirements for developing wide division multiplexing systems, the emission bandwidths and lifetimes of the various concentrations of Er^{3+} -doped multicomponent tellurite glasses were extensively investigated. The other objective of the present exploration is to have an inclusive understanding over the dielectric and ac conductivity behaviour of the prepared multicomponent tellurite glasses. An attempt has also been made to investigate the compositional and microstructural properties of TPBKZFEr glasses fabricated by the melt quench technique.

2.   Fabrication and measurements of the glasses

For the present investigation, the glass samples were prepared from reagent grade raw materials TeO_2, KH_2PO_4, H_3BO_3, ZnF_2 and Er_2O_3 in appropriate proportions by melt quenching technique. The reagents were melted in a platinum crucible followed by adequate heat treatment according to the glass transition temperature of the composition. The glasses with molar composition (60-x) TeO_2 + 10K_2O + 10P_2O_5 + 10B_2O_3 + 10ZnF_2 + xEr_2O_3 (where, x = 0.0, 0.05 0.1, 0.3, 0.5 and

1.0 mol%) were prepared. The glass preparation details and some of the necessary theories/calculations adopted for the present investigation have been described in our previously reported work [11]. The prepared bulk glasses were crushed to fine powders and were characterized by energy dispersive spectroscopy using JEOL Model JED -2300. Infrared transmittance spectrum was recorded on a Perkin Elmer Spectrum 400 FTIR spectrometer (Shimadzu) with a resolution of 1 cm^{-1} in the range 400-4000 cm^{-1}. The micro-Raman analysis was done in the range 100-1500 cm^{-1} using a Labram-HR800 spectrometer with a resolution of 1 cm^{-1} under 514 nm line of Ar^{3+} laser excitation. Using Edinburgh instruments FLS920 spectrometer, at an excitation of 976 nm, the emission spectral range was scanned with 0.6 nm resolution. The photoluminescence (PL) lifetime was evaluated using time resolved PL spectra under 976 nm excitation, whereby the laser source was pulsed at 100 ms period and having a time resolution of 0.2 ms. The glasses were sandwiched between two platinum plated electrodes and has been applied different frequencies of sinusoidal voltages in order to carry out the dielectric measurements. The dielectric properties such as dielectric constant (ε') and loss tangent (tan δ) of the glasses were calculated from the impedance, capacitance and phase angle measurements as a function of frequency (100 Hz -1 MHz) using Agilent impedance analyzer E4980A. Efforts were also made to analyze the effect of concentration of the rare earth dopant on the conductivity and dielectric properties of the TPBKZFEr glass system at different frequencies. All the measurements were made at room temperature.

3. Results and discussion

3.1 Energy dispersive spectrum (EDS) analysis

The elemental composition present in the glass sample is analyzed through the diffraction technique with EDS analysis. The energy dispersive spectrum of 0.5 mol% Er$_2$O$_3$ -doped TPBKZF glass is shown in Fig. 1 and the observed X-ray energies have been assigned to corresponding elements. The spectrum clearly confirms the presence of expected constituent elements according to the glass composition. The main peaks corresponding to 0.53, 2.01, 3.31, and 8.63 keV represent K$_\alpha$ emissions from oxygen, phosphorus, potassium and zinc atoms, respectively. The L$_\alpha$ X-ray emissions from the tellurium and erbium atoms are obtained at energies 3.77 and 6.95 keV, respectively [12] Whereas, the elements fluorine and boron present in the glass cannot be detected by EDS because of their low range atomic numbers. The rest of the peaks in the EDS spectrum corresponding to different energies are the contributions by the K$_\beta$ and L series X-ray emissions from zinc atom, L series emissions from tellurium atom, K$_\beta$ emissions from potassium atom and finally L series and M series emissions from the erbium atom.

3.2 Vibrational modes of the glasses: FTIR and micro-Raman analysis

The IR transmittance and micro-Raman spectra of 0.5 mol% Er^{3+} -doped TPBKZF glass have been compared in Fig. 2. In this glass system, the significant IR bands were observed at 599, 923 and 1385 cm^{-1}. The prominent band around 599 cm^{-1} can be assigned to the stretching vibrations of the TeO_4 triagonal bipyramid structure [13]. The band at 923 cm^{-1} was assigned to asymmetric stretching vibrations of P-O-P groups [14] . The band around 1385 cm^{-1} is also observed in TPBKZFEr05 glass and can be attributed to the B−O⁻stretching vibrations of BO_3 units in metaborate, pyroborate and orthoborate groups [15]. The OH content in the glass system is reduced by the presence of fluorine and as a result the intensity of absorption due to the O-H group is negligible [16].

The micro-Raman scattering spectrum obtained for the TPBKZFEr05 glass in the 400–1500 cm^{-1} range has been used to recognize various structural units present in the glass matrix. The observed intense bands were identified and are summarized as follows. The band at 472 cm^{-1} can be ascribed to the symmetrical stretching or bending vibrations of the shared sites along the chains of TeO_4, TeO_3 and TeO_{3+1} [17,18]. While, the band at 668 cm^{-1} is assigned to asymmetric vibrations of the network generated by TeO_4 triagonal bypyramid (tbp) groups, which were linked through Te-O-Te, with O occupies alternative axial and equatorial positions [19]. The band around 744 cm^{-1} arises from the stretching vibrations of TeO_3 and TeO_{3+1} triagonal pyramids [20,21]. The peak position around 980 cm^{-1} can be attributed to the vibrations of pentaborate and tetraborate groups [22]. The examination of the results of IR and Raman spectral studies for the present glass under investigation reveals that, there is no development of the structural peaks of rare earth; which indicates the fine dispersion of rare earth species in the host matrix and is also a clue for the absence of cluster formation [9].

3.3 Infrared fluorescence at 1.53 μm and concentration dependent fluorescence properties

Our prior analysis and exploration illustrate that the prepared tellurite glasses have fine integrities for visible luminescence [11]. In order to accomplish erbium doped glasses for broad band and gain amplification, it is crucial to evaluate the full width at half maximum (FWHM) and stimulated emission cross-section of 1.53 μm band. With a pumping of 976 nm, Er^{3+} ions were excited from the $^4I_{15/2}$ ground state to the $^4I_{11/2}$ metastable state; from where, non-radiative decay occurs which populates the $^4I_{13/2}$ lasing level and efficient emission occurs at 1.53 μm. This emission wavelength is almost insensitive to that of the host material in which the Er^{3+} is doped, since the 4f shell is secured from its surrounding with the filled 5s and 5p shells. The NIR emission spectra of the Er^{3+} -doped tellurite glasses recorded by monitoring an excitation at 976 nm are shown in Fig. 3. As can be seen, the spectra consist of the characteristic bands originated from the $^4I_{13/2}$ meta-stable level

to the terminal $^4I_{15/2}$ level. Even if all the bands are same, centered at 1.53 μm, a significant broadening of emission with increased Er^{3+} ion concentration is clearly perceived. When the glass contains 0.5 mol% Er_2O_3, the 1.53μm fluorescence intensity of Er^{3+} reaches a maximum value, which is 3 times higher than that of lowest Er^{3+}-doped glass. Since the 1.53 μm emission in glasses are known to be of asymmetric nature, specifying effective linewidth rather than FWHM is more meaningful [23]. According to Weber, dividing the areas of emission by the corresponding peak maxima will give the effective linewidths. $\Delta\lambda_{eff} = \frac{\int I(\lambda)d\lambda}{I_{max}}$ (1)

The effective linewidths of the prepared glass series for the transition $^4I_{13/2} \rightarrow ^4I_{15/2}$ range from 54-64 nm, which are comparable with other tellurite glasses [24] and are greater than that obtained for silica-based glasses [25]. Thus it is evident that an increment in bandwidth can be achieved by tailoring the ion concentration.

From the emission spectra, luminescence quenching is manifested for the NIR emission of TPBKZFEr glasses. The intensity of emission drastically increases and has a maximum around 0.5 mol% of Er_2O_3 and then decreases with an increase in the Er_2O_3 content. As the concentration of RE species increases, upto a certain value the optical gain shows an increasing trend. Beyond which the quenching of luminescence occurs either by the formation of RE aggregates or because of the formation of optically inactive rare earth compounds/alloys with the host matrix. Inset of Fig. 3 shows the Er^{3+} content dependence of the emission intensity and the effective linewidth for the $^4I_{13/2} \rightarrow ^4I_{15/2}$ transition. The ion concentration and the composition of the glass can modify the signal intensity of the emission and also the spectral bandwidth.

Based on the measured fluorescence spectra, some important spectroscopic parameters can also be derived. The assessment of stimulated emission cross section (σ_e) is one of the central factor in order to realize the emission performance of the glass [26]. For the measured NIR emission at 1.53 μm, σ_e was evaluated by the Fuchtbauer-Ladenburg equation [27]

$$\sigma_e = \frac{\lambda_p^4 A[(S\,L)J,(S'\,L')J']}{8\pi cn^2 \Delta\lambda_{eff}}$$ (2)

where λ_p denotes the peak wavelength of the NIR emission band, $\Delta\lambda_{eff}$ is the effective linewidth, c is the velocity of light, n is the refractive index and A is the transition probability. The emission peak locates at 1.53 μm for the TPBKZFEr05 glass has effective linewidth of ~ 63 nm and stimulated emission cross- section of 9.67×10^{-21} cm^2. The broad NIR emission band with large emission cross section indicates that the series of this particular glass system are suitable materials for developing broadband optical amplifier. Figure-of-merit for bandwidth (ΔG) is also an important parameter to

evaluate the bandwidth properties of the broadband fiber amplifier and can be calculated by the equation

$$\Delta G = \Delta\lambda_{eff} \times \sigma_e(\lambda_p) \tag{3}$$

The large value of ΔG indicates the better properties suitable for optical amplifiers. Table 1 shows the comparison of the stimulated emission cross section and figure-of-merit for bandwidth for the observed NIR transition, $^4I_{13/2}{\rightarrow}^4I_{15/2}$ of the TPBKZFEr05 glass with those of other host glasses [10,33,35,49]. From which it is evident that the present glass system under examination offers promising results as compared with other literature data. Together with the broad emission from the level $^4I_{13/2}$, the glass under investigation also possesses high value of stimulated emission cross-section and ΔG, which indicate the better bandwidth characteristics and so the glasses are attractive for broadband amplifiers.

Taking radiation trapping effects into consideration, broadening of the emission band at 1.53 µm as the Er^{3+} ion concentration increase can be explained. Radiation trapping occurs in a typical 3-level system where the absorption and emission spectra overlap, just as in the case of $^5I_7 \leftrightarrow ^5I_8$ in Ho^{3+} at 2.1 µm and $^3F_4 \leftrightarrow ^3H_6$ in Tm^{3+} at 2.0 µm [28]. In the same manner, high degrees of overlap between the absorption and emission cross-sections are considered for the $^4I_{13/2} \leftrightarrow ^4I_{15/2}$ transition of Er^{3+} ions at 1.53 µm. Some of the radiatively emitted photons from the $^4I_{13/2}$ level of the Er^{3+} ion are reabsorbed by the unexcited Er^{3+} ions, which induces the $^4I_{13/2}{\rightarrow}^4I_{15/2}$ transition and subsequent emission. Since the NIR absorption and emission peaks overlap around 1.53 µm wavelength, the reabsorption around that peak is more efficient as compared to other wavelengths in Er^{3+} -doped hosts. Hence, it is inferred that as the Er^{3+} concentration increases, the measured emission intensity around the peak decreases, which leads to a bandwidth broadening [29]. The obtained Er^{3+} emission spectrum in tellurite matrix is broader than that of silicate and phosphate glasses [30,31].

The absorption cross-section (ACS) from absorption spectrum and the emission cross-section from Mccumber theory have been calculated and reported in our previous work [11]. For comparison of the line- shape and to verify the broadening nature, the absorption and emission cross-sections obtained for TPBKZFEr05 glass together with its measured fluorescence are depicted in Fig. 4. The two cross-sections are reported with the indicated scale, 10^{-21} cm^2 and the photoluminescence (PL) spectrum is reported in an arbitrary scale for comparison of line-shapes. It can be seen that the emission profile is similar while the broadening is being due to the difference attributed to reabsorption, as mentioned before.

3.3.1 The gain spectra characteristics

In the present analysis, the gain coefficient has been computed for the emission at ~1.53 μm. It is assumed that there is a simplified two level system for which the Er^{3+} ions are distributed between the ground state ($^4I_{15/2}$) and the upper state ($^4I_{13/2}$). It is possible to evaluate the net gain coefficient ($G(\lambda)$) at wavelength (λ) as a function of the fractional population at the pumping level (P) using the measured absorption cross-section (σ_a) and the emission cross-section (σ_e) by the following equation[32]

$$G(\lambda) = N[P\sigma_e(\lambda) - (1 - P)\sigma_a(\lambda)] \tag{4}$$

where P is the population inversion parameter defined as the ratio of number of active ions in the excited state Er^{3+} lasing level ($^4I_{13/2}$) to total number of active ions in the glass. N is the concentration (=1.848×10^{20} ions/cm^3) of Er^{3+} ions. The gain coefficient spectrum for TPBKZFEr05 glass has been computed as a function of wavelength using the above equation for a set of P values ranging from 0.0 to 1.0 with a step of 0.1, and the results are represented in Fig. 5. It is evident that the intensity as well as the width of the gain curve increase with the population inversion. It is also observed from the spectra that there is no shift in the peak of gain coefficient as population inversion is increased. When the ground and excited states are equally populated ($P = 0.5$), there is zero gain coefficient. For $P = 0.6$, a positive gain appears covering the spectral region from 1530 to 1630 nm (L-band). For higher values of population inversion, gain becomes positive both for the L and S bands ranging from 1430 to 1630 nm. The gain coefficient value for TPBKZFEr05 glass is comparable with previously reported erbium doped tellurite glass [33]. Thus it can be concluded that for the population inversion greater than 50%, the TPBKZFEr05 glass exhibits a gain in the region relevant for the optical communication window and provides more channels in the wavelength division multiplex (WDM) networks.

3.4   Lifetime of $^4I_{13/2}$ level of Er^{3+} ion in TPBKZFEr05 glass

In general, erbium doped tellurite glasses can have long fluorescence lifetimes compared to other erbium doped host glasses at certain pump wavelengths because of their low phonon energies [34] As the stimulated emission cross-section, lifetime of $^4I_{13/2}$ level of Er^{3+} is also an important parameter for broadband optical amplifiers or lasers at the 1.53 μm. The PL decay spectra monitored at 976 nm excitation for various concentrations of Er^{3+} ion are plotted in Fig. 6. For 0.05 mol% Er^{3+} - doped glass, the decay curve could be described by a single exponential function and it gives an idea of the absence of energy transfer among the Er^{3+} ions. The experimental lifetime (τ_{exp}) in single exponential decay, is measured by curve fitting using the equation

$$y = y_0 + Ae^{t/\tau} \tag{5}$$

where t gives the time after excitation.

For higher concentration Er^{3+} -doped glasses, the curves could be described by a non- exponential behaviour due to the cross-relaxation through multi-polar interactions between the Er^{3+} ions. The measured fluorescence decay curves for higher concentration Er^{3+} -doped glasses were fit to a double-exponential function to estimate the lifetime of $^{4}I_{13/2}$ level.

$$I(t) = A_1 \exp\left(-t/\tau_1\right) + A_2 \exp\left(-t/\tau_2\right) \tag{6}$$

$I(t)$ is the intensity of luminescence for a time, t. τ_1 and τ_2 are the short and long lifetimes corresponding to the intensity coefficients A_1 and A_2 which are the fitting parameters. The average lifetime was calculated by the equation

$$\tau_{exp} = \frac{A_1\tau_1^2 + A_2\tau_2^2}{A_1\tau_1 + A_2\tau_2} \tag{7}$$

The experimental lifetimes (τ_{exp}) of the $^{4}I_{13/2}$ level are estimated to be 4.17, 3.84, 3.75, 3.59 and 3.49 ms for the prepared multicomponent tellurite glasses doped with 0.05, 0.1, 0.3, 0.5 and 1.0 mol% of Er^{3+} ions, respectively.

Figure-of-merit (FOM) for amplifier gain (G) is an imperative parameter so as to evaluate the performance of the amplifier while designing amplifier devices. It is specified as the product of lifetime and stimulated emission cross-section.

$$G = \tau_{exp} \times \sigma_e(\lambda_p) \tag{8}$$

Corresponding to the $^{4}I_{13/2} \rightarrow ^{4}I_{15/2}$ NIR emission transition for the TPBKZFEr05 glass the value of G is found to be 34.72×10^{-24} cm^2s. This value indicates that the current glass system is potentially valuable for a laser material at 1.53 μm wavelength. In our previous paper [11] the radiative lifetime of the $^{4}I_{13/2}$ level of Er^{3+} ion in TPBKZFEr05 glass was predicted as 3.243 ms. Using the measured lifetime and radiative lifetime, the quantum efficiency was estimated for the $^{4}I_{13/2}$ metastable state of the Er^{3+} as per the equation follows

$$\eta = \frac{\tau_{exp}}{\tau_R} \times 100 \% \tag{9}$$

While calculating the quantum efficiency of TPBKZFEr05 glass, the value was found to be beyond 100%. This discrepancy is mainly caused from the fact that the self absorption introduces a delay in the excited luminescence due to successive reabsorption and re-emission processes. It influences the experimental lifetime by which reabsorption of early emitted photons lengthens the emission process inside the sample depending on the absorption cross-section(σ_a) and thickness (L). From the

Auzel's approach, the lifetime corrected for the self-absorption effect is obtained by the equation [35]

$$\tau_{exp} = \tau_{PL}(1 + \sigma_a NL) \tag{10}$$

where τ_{PL} is the non affected value of lifetime by self-absorption and N is the ion concentration. The corrected lifetime was found as 2.56 ms for $^4I_{13/2}$ level of Er^{3+} in TPBKZFEr05 glass. The comparative study on the spectral properties of the NIR emission recommends that the glass material under examination might be a promising candidate for Er^{3+}-doped fiber amplifiers.

3.5 Compositional and frequency dependent dielectric properties

3.5.1 Dielectric constant and loss tangent (ε', ε'' and $tan\ \delta$)

Examination on the dielectric properties aids in estimating the insulating strength of the glasses which enhances the comprehensive understanding of the structural aspects of the glasses. With an applied ac electric field, the response of matter can be depicted in terms of dielectric permittivity

$$\varepsilon^* = \varepsilon' + \varepsilon'' \tag{11}$$

where the real part of dielectric constant ε', gives the amount of energy stored in dielectric material as polarization and the imaginary part of dielectric constant, ε'' represents the energy loss due to polarization and ionic conduction. The dielectric permittivity, ε' of a material placed in between the conducting plates are calculated by the equation

$$\varepsilon' = \frac{CL}{\varepsilon_0 A} \tag{12}$$

where C is the capacitance of the material in the applied electric field represented in Farad, A is the cross-sectional area of the sample measured in m^2, ε_0 is the permittivity of the free space which is equal to 8.854×10^{-12} f/m and L is the thickness of the sample measured in m. The permittivity values are related to the electron density and ionic charges. The effect of frequency on dielectric constant ε' for TPBKZFEr glasses in the frequency range, 100 Hz - 1 MHz at room temperature is depicted in Fig. 7. It describes the polarizing performance of the material in the presence of applied electric field. From the plotted data, it is revealed that for the range of frequency applied, the title glasses were not illustrating any significant variation with frequency as there is no major change in the orientation of molecule and the electron exchange between the ions does not follow the variations in the applied field. For some of the selected frequencies, the real part of the dielectric constants was depicted in Fig. 8. As the concentration of the Er^{3+} ions increased, these ions disrupt the glass network by creating dangling bonds and non-bridging ions which creates comfortable pathways for the migration of charges and thus develop space charge polarization leading to the increase in

dielectric constant as observed initially. The dielectric constant increases with increase in substitution percentage of Er^{3+} and attains maximum for TPBKZFEr05 glass and then decreases for higher substitution, for the entire frequency range.

Polarization lags behind the applied electric field causing an interaction between the field and the dielectric polarization which results in dissipation of energy or dielectric loss in the form of heat. Other reasons are the impurities and the imperfections in the crystal lattice. High porosity and low density lead to low dielectric constant and dielectric loss [36]. Figure 9 exhibits the frequency dependence of dielectric loss of all the glasses. The dielectric losses for all the glasses were observed to be decreased with the increase in frequency of the applied field. It is evident from the figure that the loss decreases rapidly in the low frequency region while the rate of decrease is slow in the middle frequency region. As the applied frequency increases, the ions are not able to respond quickly and it reveals an almost frequency independent behaviour in the high frequency region. This is due to the combination of both ion jump and conduction loss. The maximum values of $\tan \delta$ are noticed in the frequency range from 100 Hz - 10 kHz for all the glasses. The loss peak, which is the characteristic of low loss materials [37], did not shown by the present glasses in the 100 Hz – 1 MHz range. The dielectric loss factor depends on a number of factors such as stoichiometry and structural homogeneity which in turn depends upon the composition. The inset of Fig. 9 shows the Er^{3+} concentration dependence of quality factor [38] $\left(Q = \frac{1}{\tan\delta} \right)$ at a frequency of 1 kHz. With the increase in concentration, it is observed that upto 0.5 mol%, $\tan \delta$ shows a decreasing trend for all the doped glasses. The minimal value of dielectric loss and so the maximum quality factor is observed for 0.5 mol% Er^{3+} -doped tellurite glass.

The complex dielectric constant ε'' was calculated using the following relation

$$\varepsilon'' = \varepsilon' \tan \delta \tag{13}$$

At low frequency range, the value of ε'' increases due to the contribution of the ionic conductivity. Maximum ε'' corresponds to the maximum conversion from electromagnetic energy to thermal energy. The calculated imaginary part of dielectric constants was depicted in Fig. 10.

The break down strength of the dielectric material has an inverse relation with the specific dielectric loss (W/m^3) represented by [39]

$$\rho_1 = E^2 \omega \varepsilon_0 \varepsilon'' \tag{14}$$

It is desirable to reduce the dielectric loss across the material about which the voltage is applied so as to obtain lower ε'' value, in order to minimize the specific dielectric loss. In this sense, it is evident from figure 10 that the TPBKZFEr05 glass is having the lowest specific dielectric loss and the highest breakdown strength than other glasses and in turn shows better insulating strength.

3.5.2 AC conductivity (σ_{ac})

The ac conductivity was determined from the dielectric parameters by the relation

$$\sigma_{ac} = \omega\varepsilon'\varepsilon_0 tan\delta \tag{15}$$

where ω is the angular frequency of the electrical signal [40]. Figure 11 depicts the ac conductivity as a function of frequency at room temperature. In disordered solids, the ac conductivity is an increasing function of frequency [41]. For the total conductivity, the different characteristic regions of frequency can be distinguished according to the following relation [42].

$$\sigma_T(\omega) = \sigma_0 + \sigma_{ac}(\omega) \tag{16}$$

The frequency independent term is the dc conductivity (σ_0) which is due to band conduction; the frequency dependent function, the second term is purely ac conductivity due to the hopping process. The first term predominates at high frequency and at high temperature, while the second term is predominant at high frequency and at low temperature. The second term $\sigma_{ac}(\omega)$, ac conductivity follows the super linear power- law at higher frequencies.

$$\sigma_{ac}(\omega) = A\omega^s \text{ with } s \leq 1 \tag{17}$$

where A is a constant independent of frequency, but depends on temperature, s is a frequency exponent and ω is the angular frequency($\omega = 2\pi f$). This equation is valid for several low mobility amorphous and even crystalline materials[43]. The plot between log f and σ_{ac} shows two distinct regions. At low frequencies, about upto 10 KHz, frequency independent plateau region is observed and it is the true bulk conductivity of the glasses. It is related to the accumulation of ions due to the slow periodic reversal of the electric field. Further at higher frequencies, frequency dispersion is observed, which is in well accordance with the Eqs. (16) and (17). This is a typical behaviour of ionic conductors [44]. The conductivity increases from 0 to 1.53×10^{-8} $\Omega^{-1}cm^{-1}$ while the frequency varies from 100 Hz to 1 MHz. In order to figure out the frequency dependence of conductivity in the glass, the barrier hopping of bipolarons has been proposed. Using the correlated barrier-hopping model (CBH), it is inferred that the electrons hopping over the Coulombic barrier between charged defects D+ and D−. The transfer is dominated at high frequencies by the contribution from hopping infinite cluster.

Conductivity is sensitive to the structure as the structure determines both the potential barriers for the transport of mobile ions and the mobile ion concentration. Also, the structure is modified by the variation of constituent elements [45]. It is clearly seen from the plot that the conductivity remains constant at low frequencies for all the concentrations. We have obtained the lowest conductivity for the 0.5 mol% of Er^{3+} concentration among all glasses under inspection within the studied frequency range and beyond this concentration, the conductivity is showing a reverse

trend, and it increases. The slope of the linear fit of the data $ln\sigma_{ac}$ versus $ln\,\omega$, gives the exponent s. The numerical values of s at room temperature for all the glasses fall in the range $0.71 < s < 0.97$ and these values are strongly indicating the carrier transport hopping of electrons. The close proximity of s to unity is regarded as the correlation with the intrinsic lattice responses arises due to the incorporation of rare earth metal ions [46] The strength of polarizibility is determined by the term A [47]. The values of σ_0, s and A are calculated for different concentrations of Er^{3+} and are given in the Table 2.

By tailoring the Er^{3+} ion concentration in the glass matrix, substantial tuning of the dielectric properties can be achieved. With respect to change in Er^{3+} concentration, the dielectric constant and dielectric loss show entirely anomalous behaviour. The similar dielectric characteristics are reported earlier too [48]. From the permittivity value of the currently investigated amorphous glass system, it is clear that the dielectric mechanism which contributes to the dielectric behaviour is due to the electronic and ionic polarizations. It is evident from the dielectric analysis that the optimal Er^{3+} doping with high dielectric constant and low loss is 0.5 mol% among all the other doping percentages.

3.5.3 Impedance studies

The impedance is of complex nature and having real and imaginary terms. By making use of complex impedance method, the bulk conductivity of the TPBKZFEr glasses can be measured. Real (Z') and imaginary (Z'') parts of impedance are given by

$$Z' = |Z|\,cos\,\theta \tag{18}$$

and

$$Z'' = |Z|\,sin\,\theta \tag{19}$$

where θ is the phase angle and is given by

$$tan\theta = \frac{Z''}{Z'} \tag{20}$$

Complex impedance data of all the TPBKZFEr glasses are presented in Fig. 12 as Cole-Cole plots and from which it is possible to derive the values of R_b, C_b and τ known as Cole-Cole parameters. The impedance plot for which Z' (real part of impedance) is against the Z''(imaginary part of impedance) appeared in the form of semicircles for various erbium ion concentrations and the centre of the semicircle is lying below the Z' axis. The semicircle starts from the origin and makes an angle $\pi/2$ with the Z' axis. The bulk resistance (R_b) values are derivable from the semicircle's intercepts on the x-axis; and the bulk capacitance values are derived from the expression which involves the frequency at the peak of the semicircle.

$$\omega_{max} = \frac{1}{2\pi f_p} \tag{21}$$

$$\omega_{max} R_b C_b = 1 \tag{22}$$

$$C_b = \frac{1}{R_b \omega_{max}} \tag{23}$$

From the Cole-Cole diagrams, the values of ω_{max} (the frequency at which the period of external electric field matches with time of relaxation of dipole) are also determined.

$$\tau = R_b C_b = \frac{1}{\omega_{max}} \tag{24}$$

where f_p is the peak frequency, R_b is the bulk resistance, C_b the bulk capacitance and τ the relaxation time. The complex impedance plots indicate the presence of ionic contribution to the electrical conductivity of these glass materials. The Cole-Cole diagram of the investigated glassy samples exhibit similar behaviour where all plots show a single semicircle which specifies a single relaxation process and the Cole-Cole parameters obtained are shown in Table 3.

4. Conclusions

Er^{3+} -doped (0.05 - 1.0 mol%) multicomponent tellurite glasses were prepared, characterized and investigated their peculiar effects on dopant concentration. From the evaluation of EDS data, various compositional elements present in the glass matrix are detected. FTIR spectra in the middle infrared region compared with the Raman spectra to facilitate structural understanding of the glass by the identification of various vibrational bands. The NIR fluorescence properties like linewidths ($\Delta\lambda_{eff}$) and lifetimes (τ_{exp}) of TPBKZFEr glasses have been studied for different Er^{3+} concentrations and the phenomenon of self- absorption has been evoked to describe the broadening of $^4I_{13/2} \rightarrow {}^4I_{15/2}$ transition. The spectroscopic parameters σ_e, ΔG, η, G, W_{NR} and $G(\lambda)$, for the transition $^4I_{13/2} \rightarrow {}^4I_{15/2}$ (1534 nm) of the 0.5 mol% Er^{3+} -doped glass, were also presented. This broad emission together with the high values of the stimulated emission cross-section and lifetime of $^4I_{13/2}$ level make these glasses attractive promising host materials for 1.53 μm broadband amplifiers in the third telecommunication window. We have also reported the effect of applied electric field frequency and composition on the dielectric properties ε', $tan\delta$ and the ac conductivity σ_{ac} of all the prepared melt quench TPBKZFEr glasses in the frequency range (100 Hz - 1 MHz). An analysis of the real and imaginary parts of impedance is performed assuming the ideal Debye behaviour as rationalized by the Cole-Cole plot. An effective tuning of dielectric constant can be accomplished by modifying the concentration of Er^{3+} ions. There is considerable improvement on the insulating performance of TPBKZFEr glasses when Er_2O_3 concentration is about 0.5 mol% in the glassy system, hence these

are more advantageous than Er^{3+} undoped glass and this appreciable results point towards the scope of development of effective materials for device fabrication to be used in various applications.
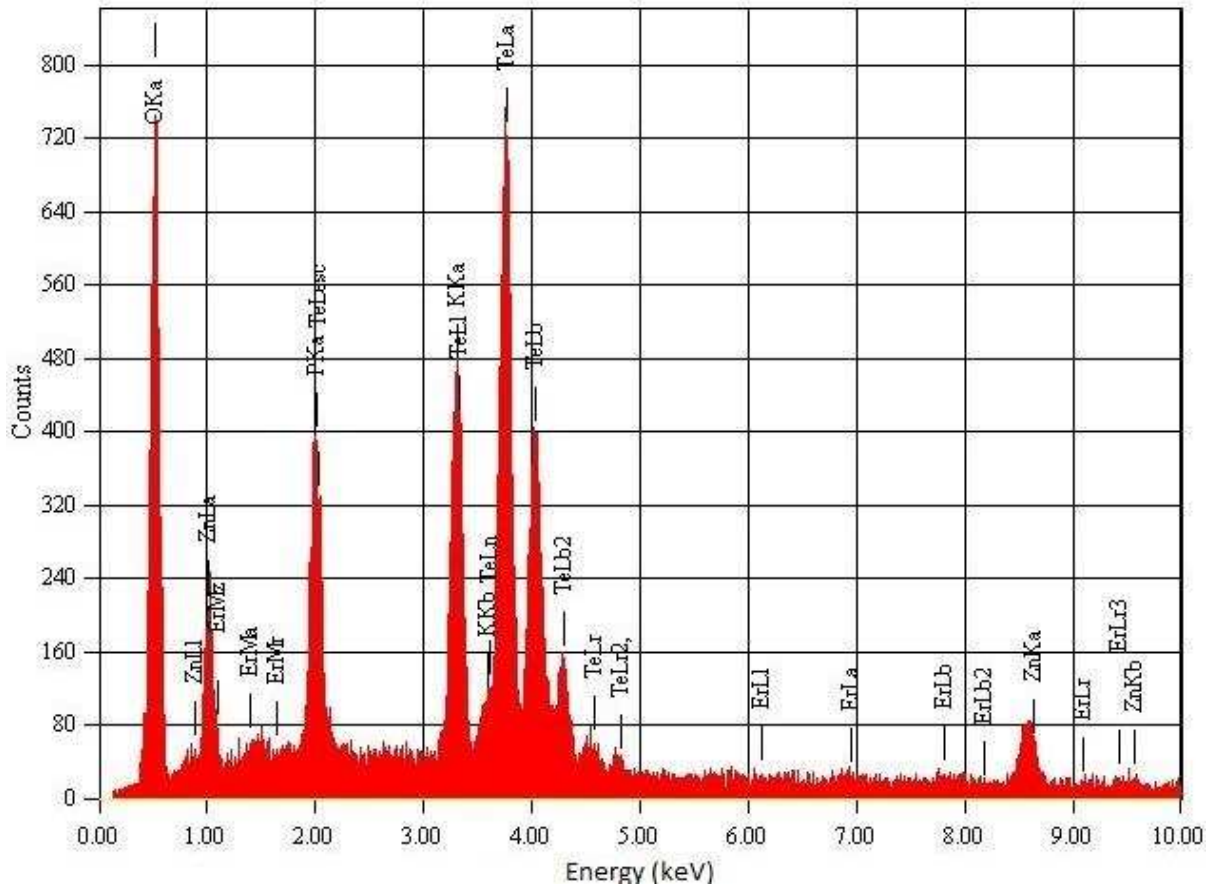
Acknowledgements

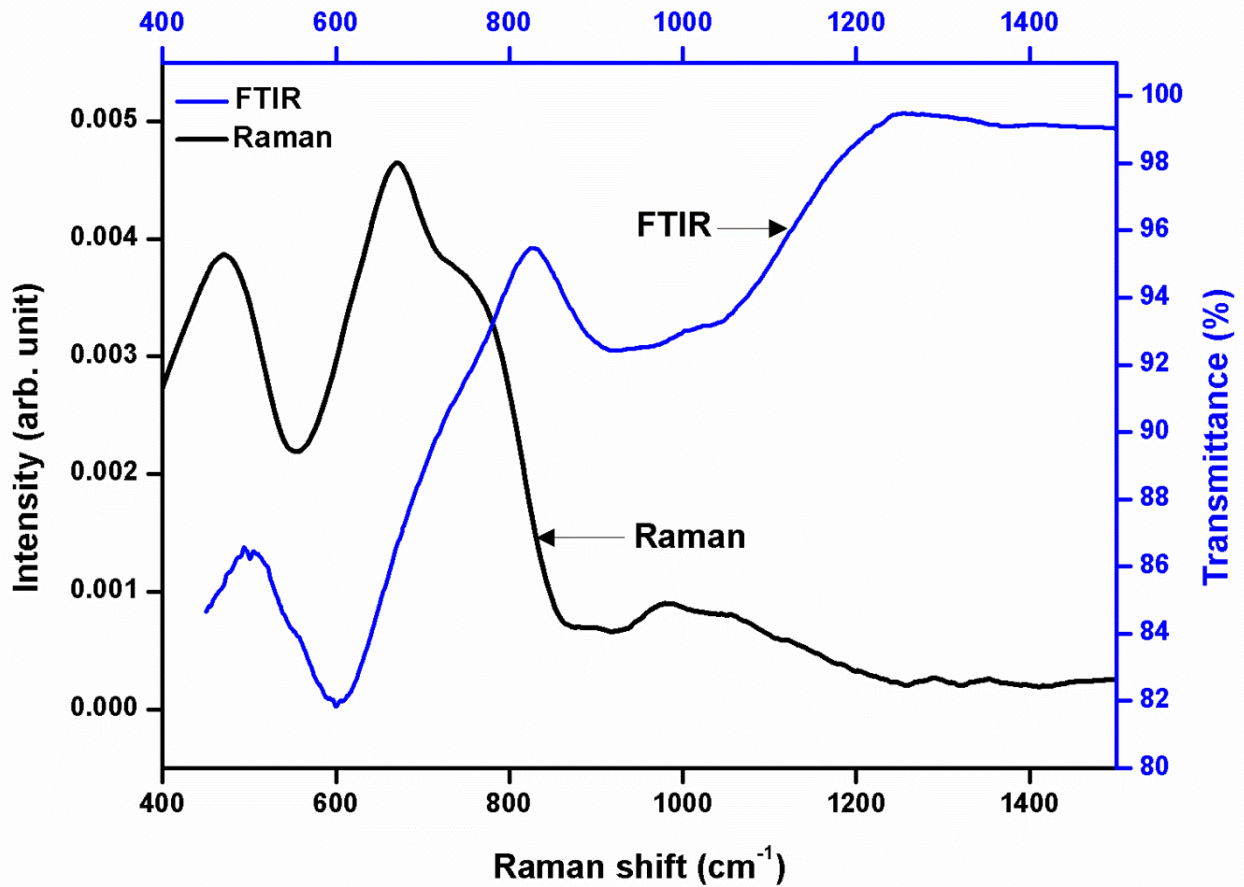Fig. 1. Energy dispersive spectrum of the TPBKZFEr05 glass.

Fig. 2. FTIR and micro-Raman spectra of 0.5 mol% Er_2O_3 -doped TPBKZF glass.

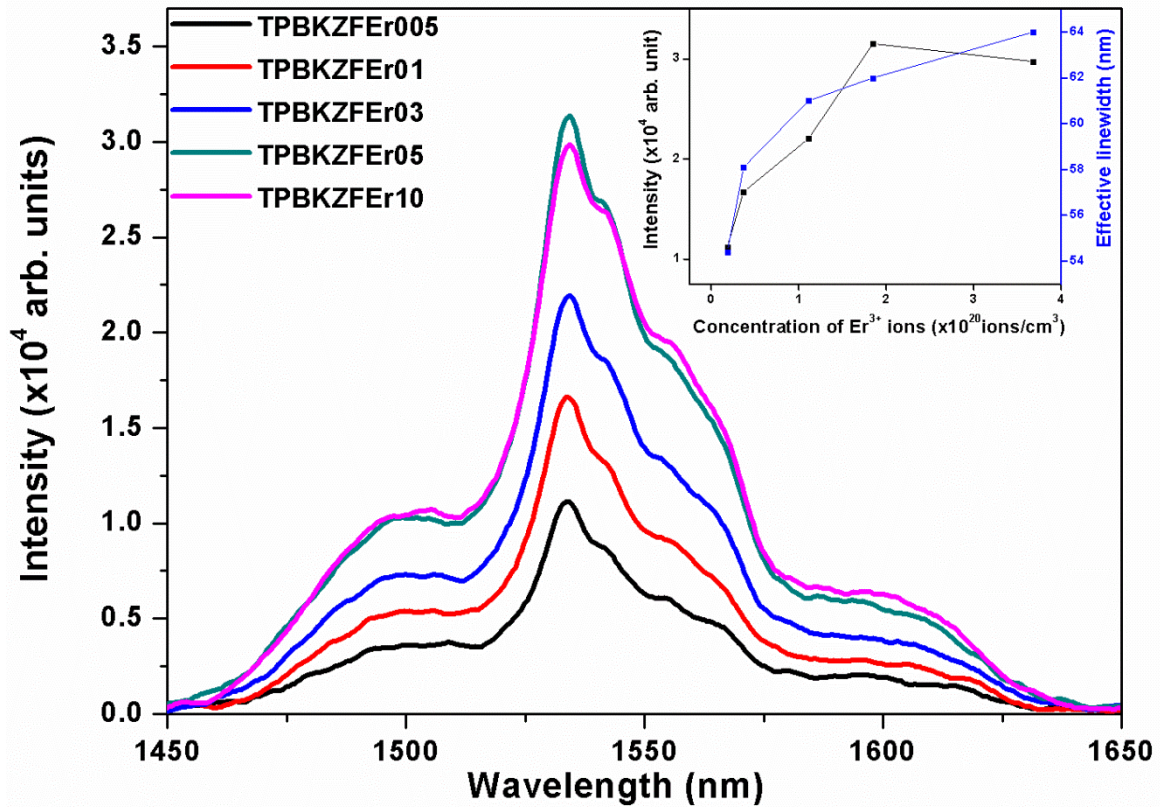Fig. 3. Emission spectra of the TPBKZFEr glasses for the $^4I_{13/2} \rightarrow\,^4I_{15/2}$ transition of Er $^{3+}$ ion upon 976 nm excitation. Inset: The dependence of Er^{3+}: 1.53 μm emission on the Er_2O_3 content.
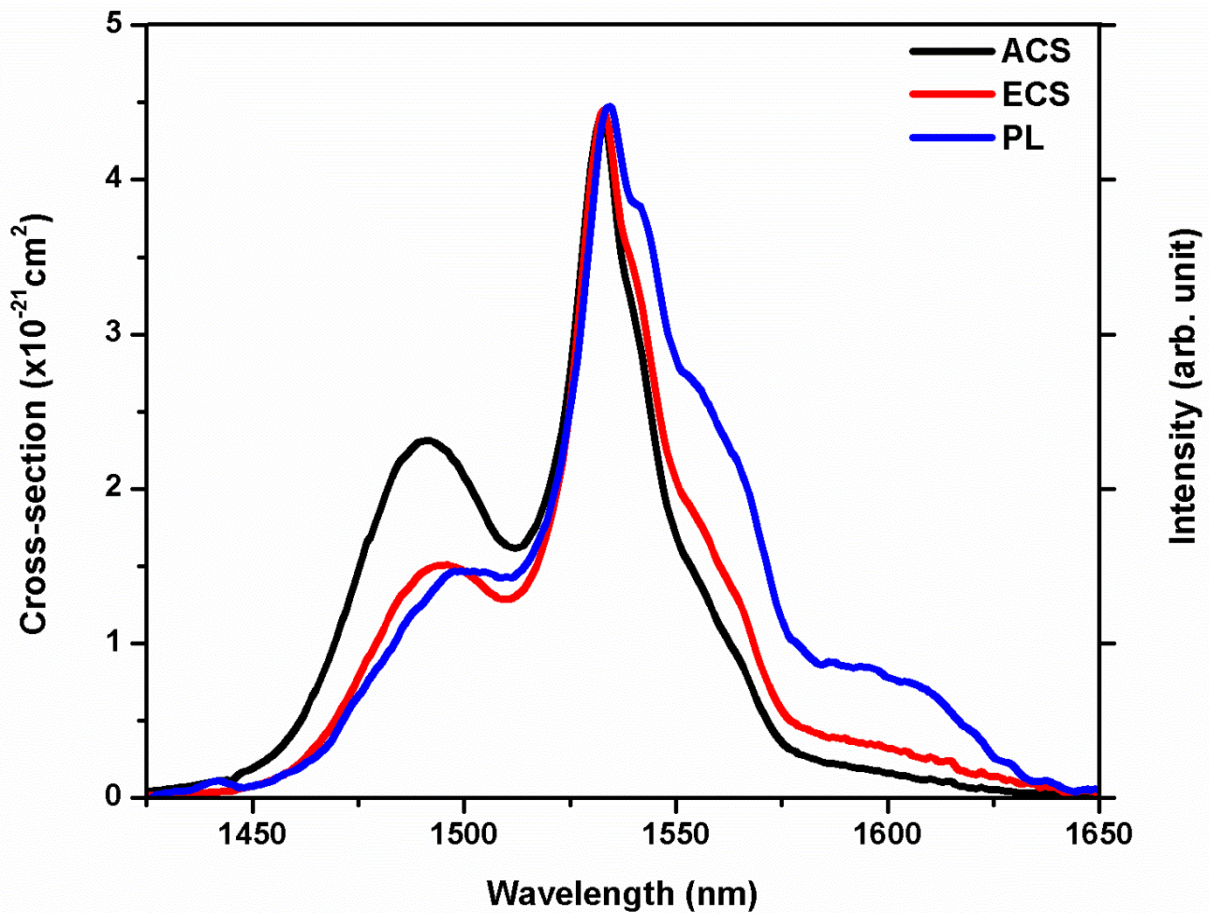

Fig. 4. Absorption and emission cross-sections of the $^4I_{13/2} \leftrightarrow\,^4I_{15/2}$ transitions for TPBKZFEr05 glass along with the measured photoluminescence (PL) spectrum.
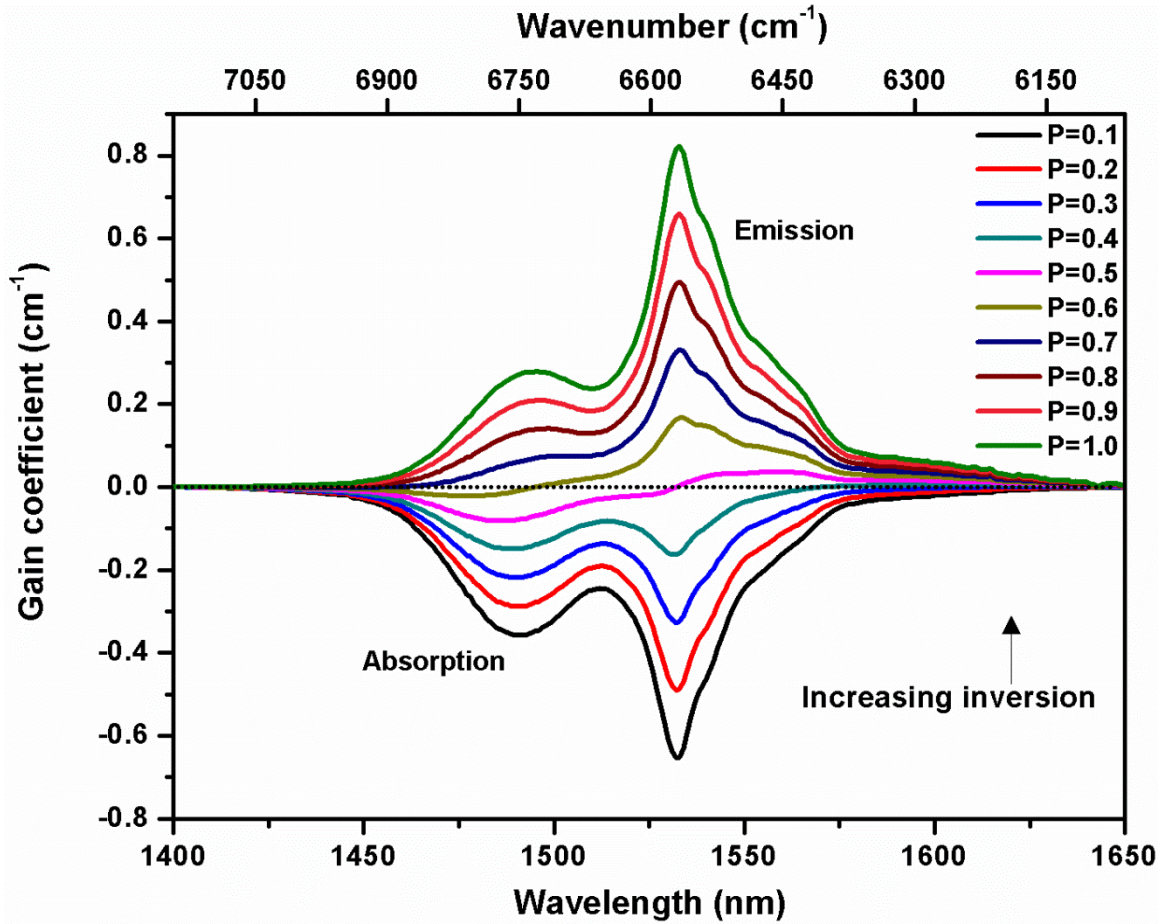
Fig. 5. Gain spectra of $^4I_{15/2} \leftrightarrow {}^4I_{13/2}$ (Er^{3+}) transitions of the TPBKZFEr05 glass as a function of population inversion parameter P.
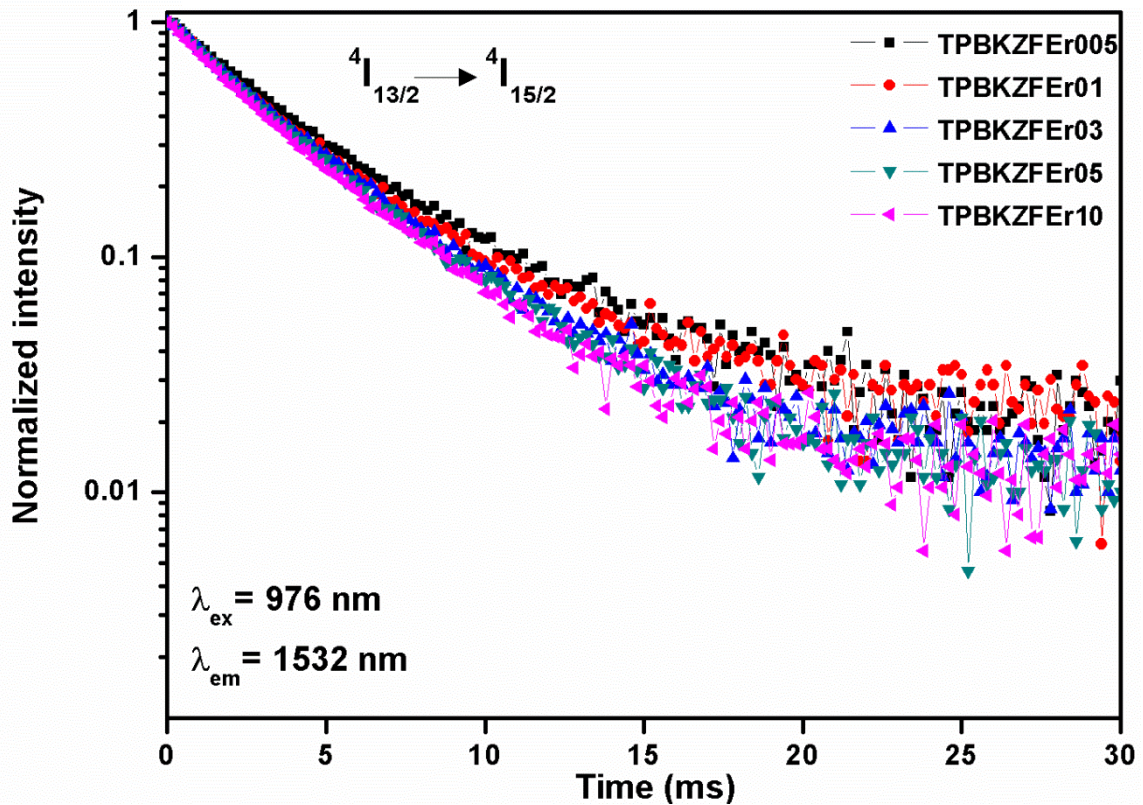

Fig. 6. Room temperature luminescence decay curves of $^4I_{13/2}$ state of the TPBKZFEr glasses at 976 nm excitation.
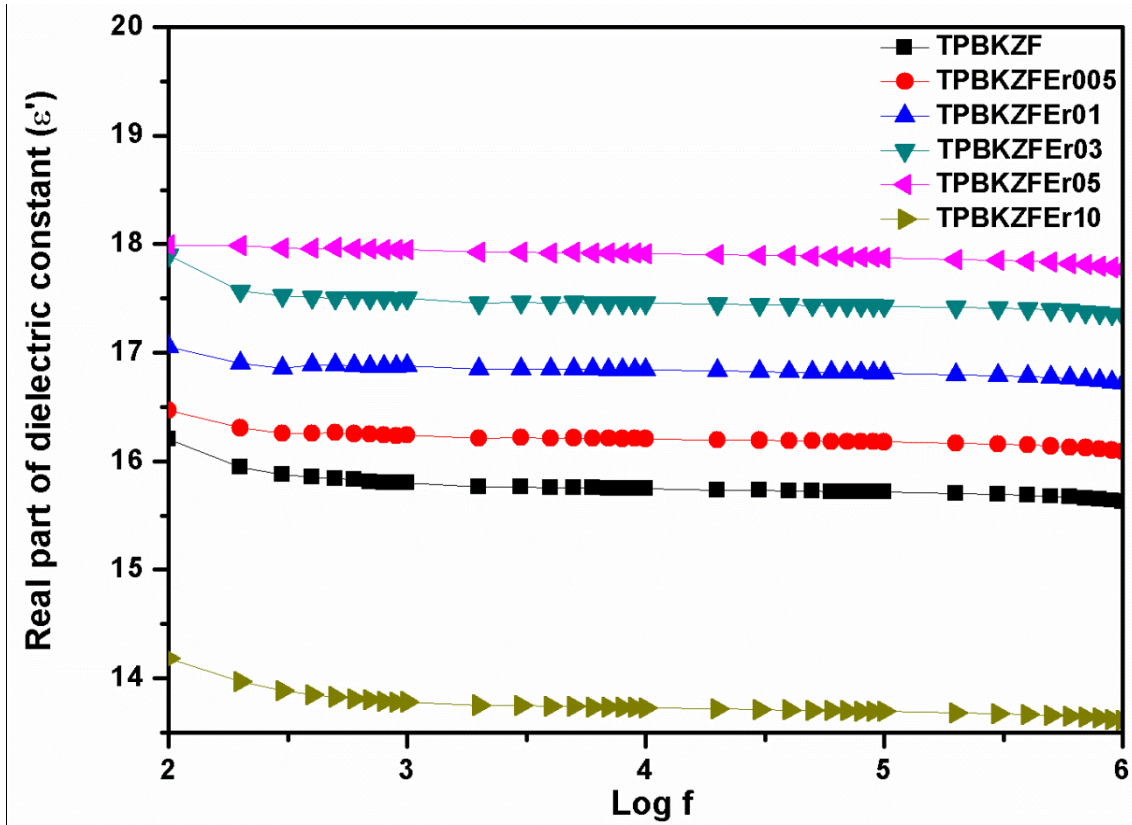
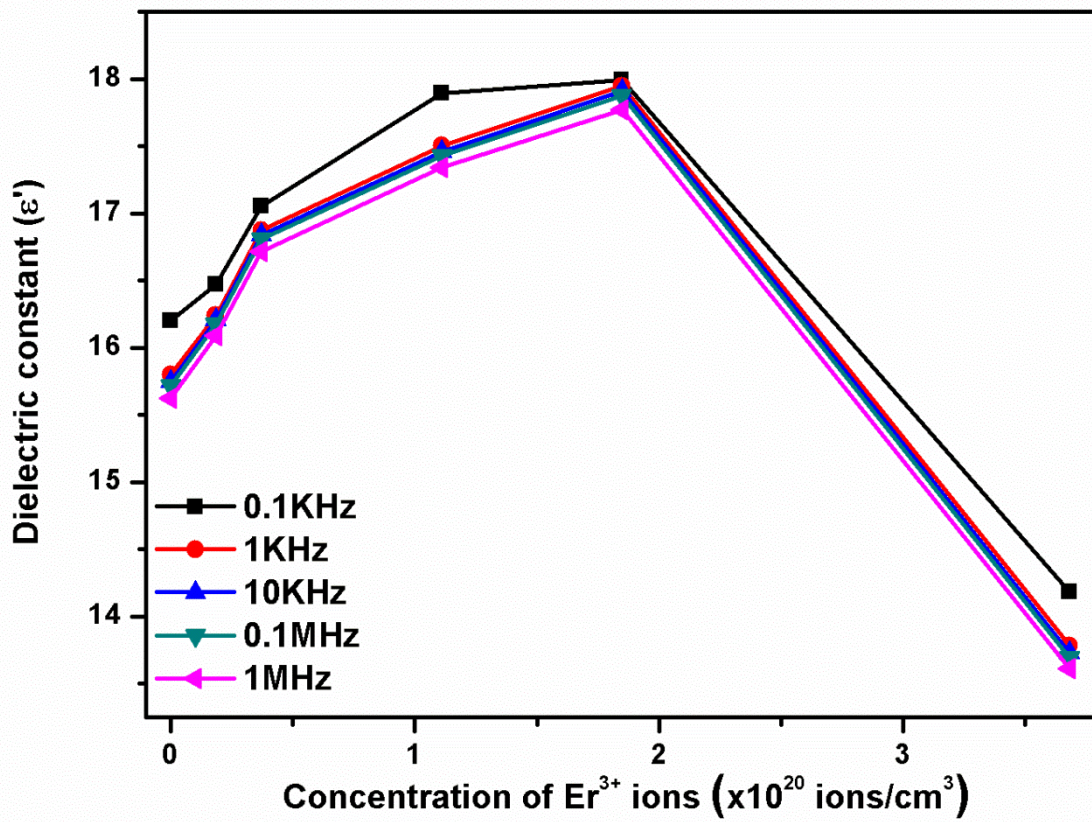Fig. 7. The frequency response of the dielectric constant for TPBKZFEr glasses.

Fig. 8. Variation of ε' with Er^{3+} ion concentration at selected frequencies.
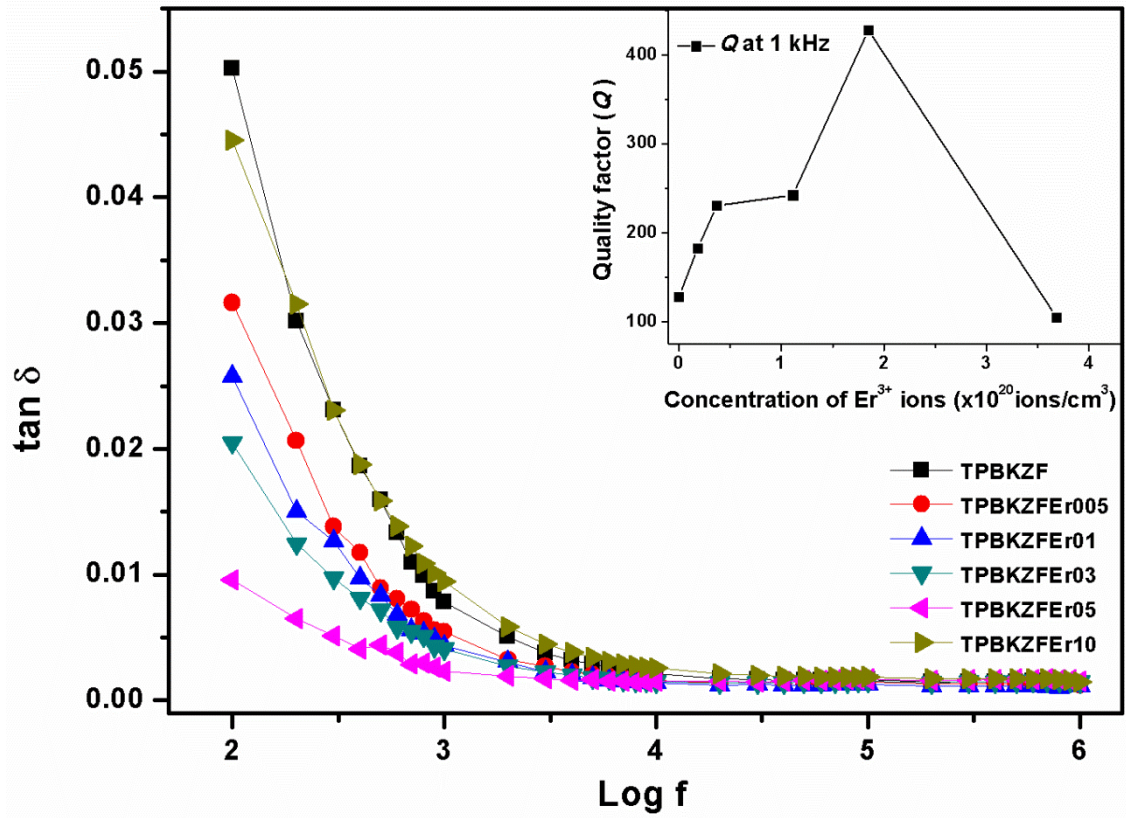
Fig. 9. Dielectric loss factor as a function of frequency for the TPBKZFEr glasses.
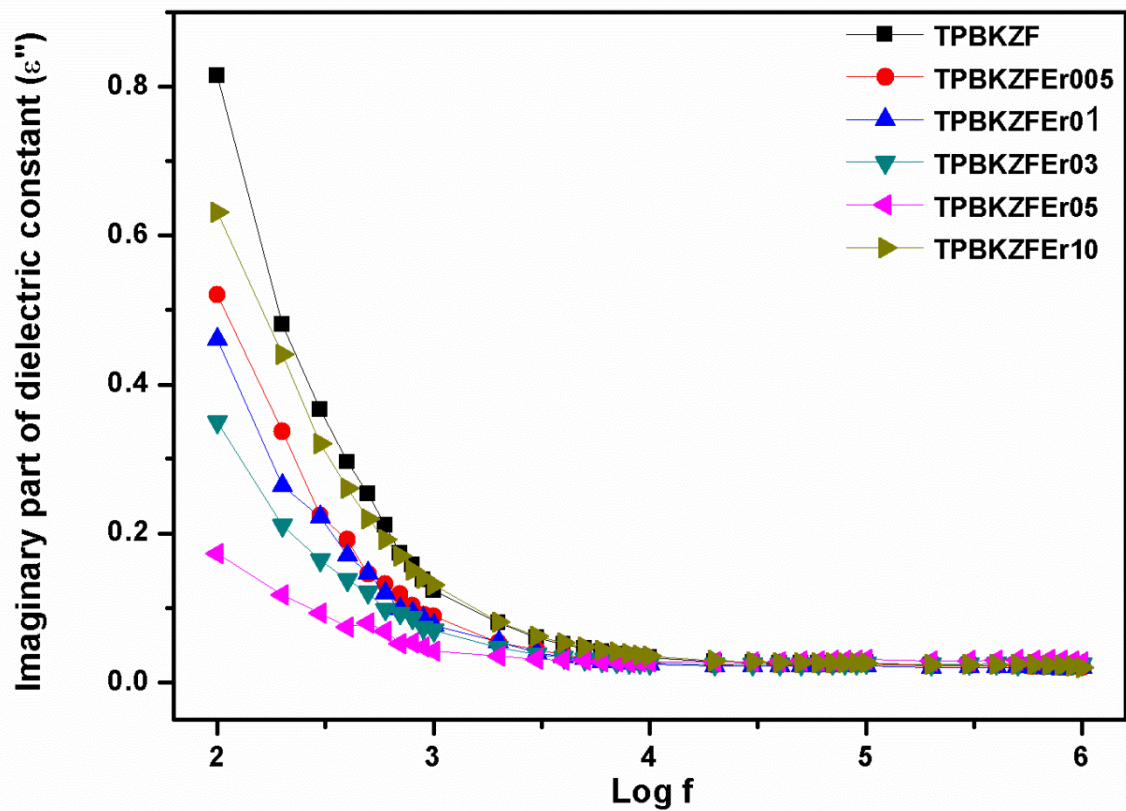
Inset: Er^{3+} concentration dependence of quality factor.

Fig. 10. Variation of imaginary part of dielectric constant with log f in Er^{3+} -doped TPBKZF glass
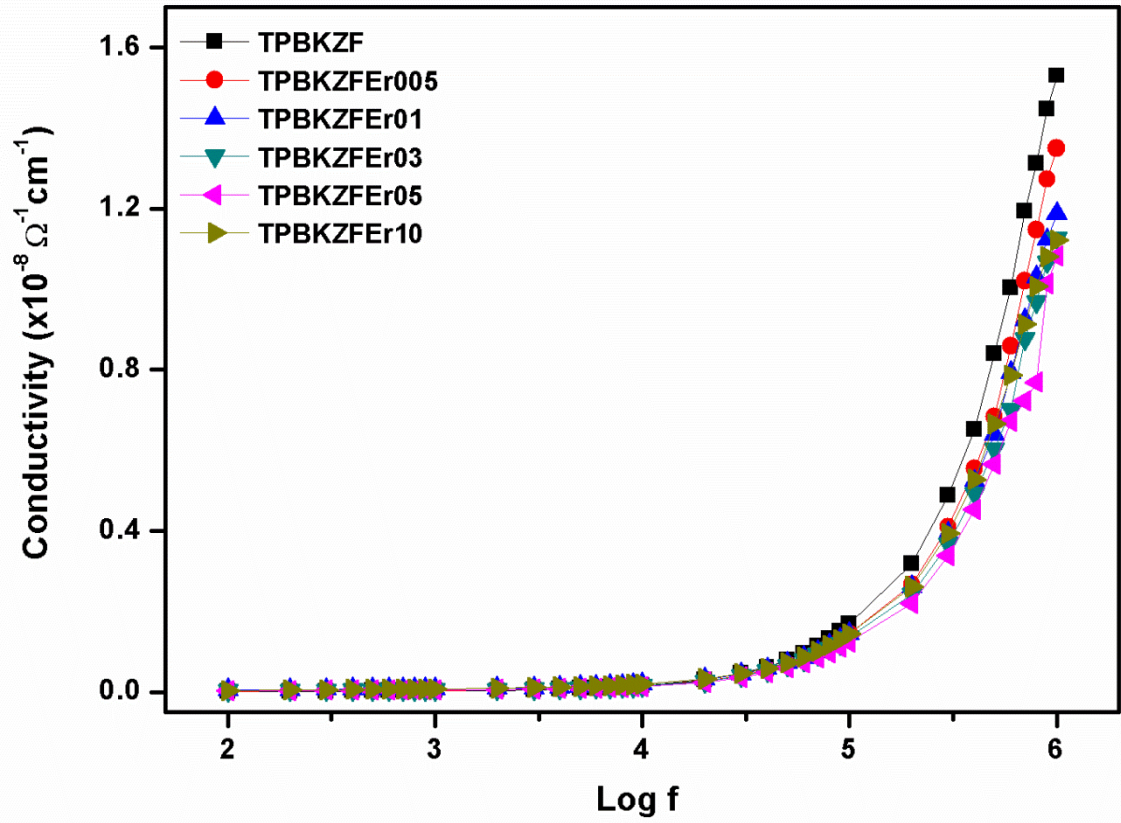
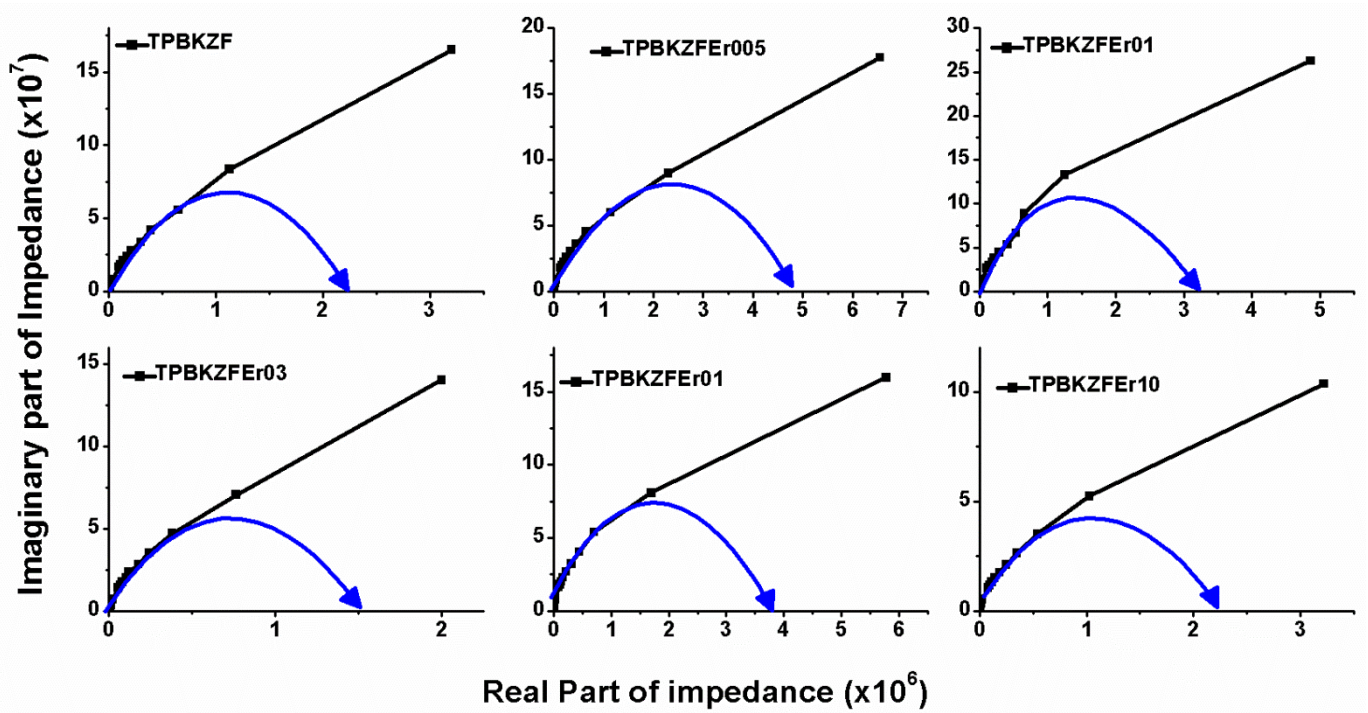Fig. 11. Electrical conductivity measured at room temperature as a function of rare earth content in TPBKZFEr glasses.

Fig. 12. Cole-Cole diagram for the complex impedance characteristics of Er^{3+}:TPBKZF glasses.

Table 1 Comparison of effective linewidths ($\Delta\lambda_{eff}$), stimulated emission cross-sections (σ_e) and ΔG for the $^4I_{13/2} \rightarrow {}^4I_{15/2}$ transition of TPBKZFEr05 glass with the other host glasses.

Glass code	$\Delta\lambda_{eff}$ (nm)	σ_e ($\times 10^{-21}$ cm^2)	ΔG ($\times 10^{-28}$ cm^3)	Reference
TPBKZFEr05	63	9.67	609.21	Present work
PBSEr(38/62)	65	5.7	370.5	[10]
LTBE0.5Y	80	5.9	472	[33]
TZF16-0.5	67.7	8.2	555	[35]
TZF35-0.5	66.7	7.1	474	[35]
TPEr	58.7	6.9	405.03	[49]

Table 2 Power-law parameters for Er^{3+}: TPBKZF glasses.

Glass code	σ_0 ($\times 10^{-11}$)	s	A ($\times 10^{-14}$)
TPBKZF	4.1441	0.7082	5.2527
TPBKZFEr005	2.5025	0.8593	1.6517
TPBKZFEr01	2.3466	0.8782	1.1177
TPBKZFEr03	1.7590	0.9193	0.7766
TPBKZFEr05	0.7917	0.9701	0.4082
TPBKZFEr10	2.9484	0.7843	5.4379

Table 3 Cole-Cole parameters for Er^{3+}: TPBKZF glasses.

Glass code	R_b (MΩ)	C_b (pF)	τ (μs)
TPBKZF	1.9359	0.2542	0.4921
TPBKZFEr005	4.0040	0.1171	0.4690
TPBKZFEr01	3.6028	0.1212	0.4368
TPBKZFEr03	1.6282	0.2527	0.4115
TPBKZFEr05	3.5122	0.1156	0.4059
TPBKZFEr10	2.2010	0.2037	0.4484

References

1. Xian Feng, Wei H. Loh, Joanne C. Flanagan, Angela Camerlingo, Sonali Dasgupta, Periklis Petropoulos, Peter Horak, Ken E. Frampton, Nicholas M. White, Jonathan H. Price, Harvey N. Rutt, and David J. Richardson, Opt. Express 16, (2008) 13651-13656.

2. Edmund Pawel Golis, Manuela Reben, Jan Wasylak, Jacek Filipecki, Optica Applicata 38 (2008)163-169.

3. Enrico Chierici, Maria Cristina Didavide, Andrea Moro, Oriana Rossotto, Luigi Tallone, lena Monchiero Fibre and Optical Passive Components, 2002. Proceedings of 2002 IEEE/LEOS Workshop 24 (2002) 28.

4. Manzani, Danilo and Ferrari, Jefferson Luis and Polachini, Ferminio Cesar and Messaddeq, Younes, Ribeiro, Sidney Jose Lima, J. Mater. Chem., 22(2012) 16540-16545.

5. A.J. Kenyon, Progr. Quantum Electron. 26 (2002) 225.

6. R.A.H. El-Mallawany, Tellurite Glasses Handbook: Physical Properties and Data, second ed., CRC Press LLC, USA, 2002.

7. B. Burtana, M. Rebenb, J. Cisowskia, J. Wasylakb, N. Nosidlaka, J. Jaglarza, B. Jarząbek, ACTA PHYS POL A, Optical and Acoustical Methods in Science and Technology120 (2011) 4.

8. P. Thomas, B.R. Varma, J. Adv. Dielectr., 2 (2012) 1250020.

9. L.M. Fortes, L.F. Santos, M. Clara Goncalves, R.M. Almeida, M. Mattarelli, M. Montagna, A. Chiasera, M. Ferrari, A. Monteil, S. Chaussedent, G.C. Righini, Opt. Mater. 29 (2007) 503–509.

10. J.A. Capobianco, G.Prevost, P.P Proulx, P. Kabro, M.Bettinelli, Opt.Mater. 6(1996)175-184.

11. M.S. Sajna, Sunil Thomas, K.A. Ann Mary, Cyriac Joseph, P.R. Biju, N.V. Unnikrishnan, Journal of Luminescence159(2015)55–65.

12. J. A. Bearden, Rev. Mod. Phys. 39 (1967) 78-124.

13. A.D Lefterova, P.V Angelov, Phy.Chem Glasses 41(2000)192.

14. G. Upender, J. Chinna Babu, V. Chandra Mouli, Spectrochemica Acta Part A 89(2012)39-45.

15. I. Arul Rayappan, K. Marimuthu, Journal of Physics and Chemistry of Solids 74 (2013) 1570–1577.

16. M.D. O'Donnell, C.A. Miller, D. Furniss, V.K. Tikhomirov, A.B. Seddon, J. Non-Cryst. Solids 331 (2003) 48–57.

17. J.S. Wang, E.M. Vogel, E. Snitzer, Opt. Mater. 3 (1994) 187.

18. A. Jha, S. Shen, M. Naftaly, Phys. Rev. B 62 (2000) 6215.

19. A.P. Caricato, M. Fernández, M. Ferrari, G. Leggieri, M. Martino, M. Mattarelli, M. Montagna, V. Resta, L. Zampedri, R.M. Almeida, M.C. Conçalves, L. Fortes, L.F. Santos, Materials Scieunce and Engineering B105 (2003) 65–69.

20. P. Charton, P. Armand, J. Non-Cryst.Solids 333 (2004)307.

21. L. Fortes, L.F. Santos, M.C. Gonc-alves, R.M. Almeida, J.Non-Cryst.Solids352 (2006) 690.

22. S. Arunkumar, K.V. Krishnaiah, K. Marimuthu, Physica B 416 (2013) 88–100.

23. M.J Weber, J.E. Lynch, D.H. Blackburn, D.J Cronin, IEEE J.Quantum .Electron.(QE-19)(1983) 600.

24. Y.Ding,S.Jiang, B.Hwang,T.Luo, N.Peyghambarian,Y.Miura, Proc. SPIE 3622(2000)166.

25. Y. Ding, S. Jiang, B.C. Hwang, T. Luo, N. Peyghambarian, Y. Himei, T. Ito, Y. Miura, Opt. Mater. 35 (2000) 123.
26. J.G. Edwards, Nature 212(1966)752.
27. J.Song, J.Heo, J.Appl.Phys.93(2003)9441.
28. P.R Ehrmann, J.H Campbell,J.Am. Ceram. Soc. 85(2002) 1061.
29. X.Feng, S. Tanabe, T. Hanada, J.Am.Ceram.Soc 84(2001)165.
30. ZhouQ, LiC, LiuZ, LiS, SongC. Multiband spectral characteristics of Er3+/Yb3+ co-doped silicate glass samples. JPhoton 37(2008)813–7.
31. Rivera-López F, Babu P, Jyothi L, Rodríguez-Mendoza U R, Martín I R , Jayasankar C K , Er^{3+}/Yb^{3+}codoped phosphate glasses used for an efficient 1.5 μm broad band gain medium.Opt.Mater 34 (2012)1235–40.
32. E. Desurvire, Erbium Doped Fiber Amplifiers: Principles and Applications, John Wiley, NewYork, 1994.
33. K. Annapoorani, K.Maheshvaran, S.Arun Kumara, N.Suriya Murthy, TeroSoukka, K. Marimuthu, Physica B 457(2015)66–77.
34. Shixun Dai, Jialu Wu, Junjie Zhang, Guonian Wang, Zhonghong Jiang, Spectrochimica Acta Part A 62 (2005) 431–437.
35. A. Miguel, R. Morea, J. Gonzalo, M.A. Arriandiaga, J. Fernandez, R. Balda, Journal of Luminescence 140 (2013) 38–44.
36. R.V. Mangalaraja, P. Manohar, F.D. Gnanam, J. Mater. Sci. 39, 2037 (2004).
37. A.K. Jonscher, A.K. Jonscher (Eds.), Solids, Chelsea Dielectric, Press, London, 1983.
38. S. Bindra, Narang, S. Bahel, J.Ceram. Process. Res. 11(2010)316-321.
39. G.N. Raju, N. Veeraiah, G. Nagarjuna, P.V.V. Satyanarayana, Physica B. 373(2006) 297-305.
40. Sunil Thomas, Sk. Nayab Rasool, M. Rathaiah, V. Venkatramu, Cyriac Joseph, N.V. Unnikrishnan, Journal of Non-Crystalline Solids 376 (2013) 106–116.
41. Jonscher AK. Nature 1977; 267:673.
42. H. Bottger, V.V. Bryksin, Hopping Conduction in Solids, Berlin, 1985.
43. N.F. Mott, E.A. Davis, Elect. Proces., in: Non Cryst Mater., Clarendon Press, Oxford, 1971/1979.
44. C.A. Angell, Solid state ionics 9-10(1983)3-741.
45. A. Languar, N. SdiriH. Elhouichet, M. Ferid, Journal of alloys and compounds 590(2014)380-387.
46. M. Careem, A. Jonscher, Phillos. Mag. 35 (1977) 6.
47. B. Louati, F. Hlel, K.Guidara, J,Alloyscomp. 486(2009)299-303.
48. M. J. Iqbal , Z. Ahmad, Journal of Power Sources 179 (2008) 763–769.
49. P. Nandi, G. Jose, Optics communications 265(2006)588-593.